Tetranuclear and Dinuclear Cu(II) Complexes with Risedronate as *anti-Trypanosoma cruzi* and *anti-Leishmania mexicana* Agents. Synthesis, Crystal Structures, and Biological Evaluation

Miguel Á. Romero-Solano,[a] Eya Caridad Rodríguez-Pupo,[b] Ignacio Martinez,[b] Berenice Prestegui-Matel,[b] Alberto Martínez-Muñoz,[c] Bertha Espinoza,[b]* Diego Martínez-Otero,[ad] Víctor López-Guerrero,[a] Alma Esteban Covarrubias[a] and Alejandro Dorazco-González.[a]*

[a] Institute of Chemistry, National Autonomous University of Mexico, Ciudad Universitaria, Mexico City, 04510, Mexico
[b] Departamento de Inmunología, Instituto de Investigaciones Biomédicas, Universidad Nacional Autónoma de México, México City 04510, México.
[c]FS Scientia Pharma S.A de C.V. Fray Diego de La Magdalena 630, Jardín Vista Hermosa, 78270, San Luis Potosí, S.L.P. México.
[d] Centro Conjunto de Investigación en Química Sustentable, UAEM-UNAM, Carretera Toluca-Atlacomulco Km 14.5, C. P. 50200, Toluca, Estado de México, México, Instituto de Química, Universidad Nacional Autónoma de México.
Corresponding authors, e-mails: B. E.: besgu@iibiomedicas.unam.mx and A. D.-G.: adg@unam.mx

Electronic Supporting Information

General: Risedronate Sodium (Merck, ≥99), $CuCl_2 \cdot 2H_2O$ (Strem Chemicals, 99%), 4,4'-dimethyl-2,2'-bipyridyl (Aldrich (Merck), 99%), 5,5'-dimethyl-2,2'-bipyridyl (Aldrich (Merck), 98%), sodium hydroxide (Fermont, 98.7%), acetonitrile (Tecsiquim, >99.5%), methanol (Tecsiquim, ≥99.8%) were purchased and used as received. Stock solutions were prepared in distilled water unless otherwise stated.

ATR-IR spectra were recorded on FT-IR NICOLET IS-50, Thermo Fisher Scientific.

High-Resolution Electrospray Ionization (HRMS) mass with positive scan spectra for **1** and **2** were obtained with a Bruker Micro TOF II.

Elemental analyses were recorded on Thermo Scientific/Flash 2000 elemental analyzer.

EPR spectra were acquired with a Jeol JES-TE300 spectrometer operating in X-Band at 100 kHz modulation frequency at a microwave frequency of 9.4 GHz and a center field of 300 mT. Spectra of **1** and **2** were obtained in H_2O frozen matrix at 77K, crystalline samples of complexes **1** and **2** were dissolved and 100 µL of glycerol was added to avoid breaking the EPR tube. The external calibration of the magnetic field was performed using a Jeol ES-FC5 precision gaussmeter with a 5350B HP microwave frequency counter. Spectral acquisition and manipulations were performed using ES-IPRITS-TE software.

UV-Vis spectra were recorded on an Agilent Cary 100 UV-VIS spectrophotometer equipped with a thermostated cell holder at 25°C (±0.1).

log $P_{o/w}$ determination: The partition coefficients between *n*-octanol-water (log $P_{o/w}$) of the complexes **1**-**2** were determined by modification of the shake-flask method.[1-2] Briefly, equal volumes of Milli-Q water and *n*-octanol were shaken together for 6 h to allow saturation of the two phases. Solutions (2 mL) of the complexes **1**-**2** were prepared in the saturated water phase (0.75 mM), and an equal volume of *n*-octanol was added. The resulting biphasic solutions were agitated for 24 h at 37 °C. Subsequently, the mixtures were centrifuged for five minutes at 6000 rpm to allow separation.

The concentration of both phases was determined by UV-Vis spectroscopy using the UV-Vis calibration curves show in **Fig. S8**. The reported log $P_{o/w}$ value is defined as log$[\text{complex}]_{\text{octanol}}/[\text{complex}]_{\text{water}}$ and the reported values are the average of three determinations.

Molecular Docking: The .pdb file for the Ris molecule was obtained from an energy and geometry optimization performed on Gaussian with semi-empirical molecular orbitals AM1 (Austin Model 1).[3] For complexes **1** and **2**, .pdb files were prepared from the XRD data. These files were used as the input files for docking simulations.

The molecular docking analysis was carried out with the AutoDock 4.2 program.[4] Subsequently, polar hydrogen atoms and atomic partial charges were included using the AutoDock Tools 1.5.6 program. The Kollman partial charges were calculated to evaluate the electrostatic contribution of the ligand-enzyme interaction.[5] The analysis was performed using blind docking method, adjusting the grid box size to 126Å X 126Å X 126Å and using a grid point spacing of 0.375 Å. The Lamarckian genetic algorithm was used for all the docking simulations considering a randomized initial population of 100 individuals and a maximum number of energy evaluations of 1×10^7. The atomic affinity maps were generated using the AutoGrid 4.0 program. The ligand-enzyme 3D complexes were visualized and analyzed using the AutoDock Tools software considering different interactions formed in each complex and selecting those with the lowest free energy values. In this way, the key residues involved in the molecular recognition of ligands by the enzyme were identified.

[1] M. V. Baker, P. J. Barnard, S. J. Berners-Price, S. K. Brayshaw, J. L. Hickey, B. W. Skelton and A. H. White, Cationic, linear Au(I) N-heterocyclic carbene complexes: Synthesis, structure and anti-mitochondrial activity, *Dalt. Trans.*, 2006, **6**, 3708–3715.
[2]
[3] Gauss View, Version 5, Dennington, R.; Keith, T.; Millan, J. Semichem Inc.: Shawnee Mission, KS, 2009.
[4] Morris, G.M.; Huey, R.; Lindstrom, R.K.; Goodsell, D.S.; Olson, A.J. AutoDock4 and AutoDock-Tools4: Automated docking with selective.
[5] The PyMOL Molecular Graphics System, Version 1.3, Schödinger, LLC.

Table S1. Crystallographic data for the complexes **1-2.**

	1	**2**
Empirical formula	$C_{62}H_{66.67}Cl_2Cu_4N_{10}O_{15.34}P_4$	$2(C_{31}H_{33.50}Cl_{1.50}Cu_2N_5O_{7.50}P_2)$, $2.468(C_2H_3N)$,$1.39(H_2O)$
Mol. Weight / g mol^{-1}	1646.22	1803.48
Crystal system	Monoclinic	Monoclinic
Space group	$P2_1/n$	C2/c
a / Å	15.5051(6)	29.967(3)
b / Å	32.1256(13)	22.628(2)
c / Å	21.0381(8)	14.1847(13)
α / °	90	90
β / °	109.1230(10)	96.630(4)
γ / °	90	90
Volume / Å^3	9901.0(7)	9554.0(16)
Z	4	4
Density / g cm^{-3}	1.104	1.254
Temperature / *K*	100(2)	100(2)
Wavelength / Å	0.71073	0.71073
Abs. Coeff. / mm^{-1}	1.017	1.088
Θ range / °	1.881 to 27.444	1.772 to 27.445
Index ranges	-17<=h<=20, -41<=k<=41, -27<=l<=27	-38<=h<=38, -29<=k<=29, -18<=l<=18
Reflections collected	91731	61296
Max. & min. transmission	0.666, 0.746	0.691, 0.746
Data / restraints / param.	22588 / 189 / 963	<10904 / 104 / 572
Goodness-of-fit on F^2	1.068	1.031
Final *R* indices [I > 2 s (I)]	R1 = 0.0455, wR2 = 0.1234	R1 = 0.0367, wR2 = 0.1082
R indices (all data)	R1 = 0.0650, wR2 = 0.1325	R1 = 0.0420, wR2 = 0.1126
Larg. diff. peak/hole / eÅ^{-3}	1.905 and -1.732	1.132 and -0.880

Table S2. Selected bond lengths (Å) and angles (°) around Cu(II) centers in **1**.

Distances (Å) and Bond Angles (°)							
Cu1-O(5)	1.9331(18	Cu2-O(6)	1.9388(18)	Cu3-O(9)	1.9297(18	Cu4-O(10)	1.9363(19)
Cu1-O(2)	1.9581(18	Cu2-O(3)	1.9810(19)	Cu3-O(3)	2.237(2)	Cu4-O(13)	1.9510(19)
Cu1-N(2)	2.001(2)	Cu2-N(5)	1.984(2)	Cu3-N(7)	1.999(2)	Cu4-N(9)	2.001(3)
Cu1-N(3)	2.011(2)	Cu2-N(4)	1.989(2)	Cu3-N(8)	1.991(2)	Cu4-N(10)	2.003(2)
Cu1-Cl(3)	2.422(18)	Cu2-O(12)	2.259(2)	Cu3-O(12)	2.0033(19)	Cu4-Cl(1)	2.709(3)
Cu1-O(3A)	2.237(19)					Cu4-O(1A)	2.136(6)
O(5)-Cu(1)-O(2)	95.66(8)	O(6)-Cu(2)-O(3)	90.73(7)	O(9)-Cu(3)-N(8)	163.66(9)	O(10)-Cu(4)-O(13)	94.76(8)
O(5)-Cu(1)-N(2)	170.20(9)	O(6)-Cu(2)-N(5)	92.47(8)	O(9)-Cu(3)-N(7)	92.27(9)	O(10)-Cu(4)-N(9)	90.25(9)
O(2)-Cu(1)-N(2)	90.62(8)	O(3)-Cu(2)-N(5)	173.09(9)	N(8)-Cu(3)-N(7)	80.85(10)	O(13)-Cu(4)-N(9)	163.07(10)
O(5)-Cu(1)-N(3)	91.29(9)	O(6)-Cu(2)-N(4)	160.56(9)	O(9)-Cu(3)-O(12)	91.05(7)	O(10)-Cu(4)-N(10)	167.23(10)
O(2)-Cu(1)-N(3)	159.34(9)	O(3)-Cu(2)-N(4)	93.95(8)	N(8)-Cu(3)-O(12)	94.13(19)	O(13)-Cu(4)-N(10)	91.90(9)
N(2)-Cu(1)-N(3)	80.31(9)	N(5)-Cu(2)-N(4)	81.05(9)	N(7)-Cu(3)-O(12)	172.31(9)	N(9)-Cu(4)-N(10)	80.39(10)
O(5)-Cu(1)-Cl(3)	88.0(3)	O(6)-Cu(2)-O(12)	93.98(7)	O(9)-Cu(3)-O(3)	94.36(7)	O(10)-Cu(4)-Cl(1)	96.74(9)
O(2)-Cu(1)-Cl(3)	99.1(3)	O(3)-Cu(2)-O(12)	81.83(8)	N(8)-Cu(3)-O(3)	101.70(8)	O(13)-Cu(4)-Cl(1)	89.74(8)
N(2)-Cu(1)-Cl(3)	98.4(3)	N(5)-Cu(2)-O(12)	104.04(9)	N(7)-Cu(3)-O(3)	104.74(9)	N(9)-Cu(4)-Cl(1)	105.74(9)
N(3)-Cu(1)-Cl(3)	100.5(3)	N(4)-Cu(2)-O(12)	105.35(8)	O(12)-Cu(3)-O(3)	81.91(8)	N(10)-Cu(4)-Cl(1)	94.17(9)
O(5)-Cu(1)-O(3A)	93.7(3)					O(10)-Cu(4)-O(1A)	94.82(15)
O(2)-Cu(1)-O(3A)	93.8(3)					O(13)-Cu(4)- O(1A)	98.04(15)
N(2)-Cu(1)-O(3A)	93.3(3)					N(9)-Cu(4)- O(1A)	97.73(16)
N(3)-Cu(1)-O(3A)	105.2(3)					N(10)-Cu(4)- O(1A)	95.02(16)

Table S3. Selected bond lengths (Å) and angles (°) around Cu(II) centers in **2**.

Distances (Å) and Bond Angles (°)					
Cu1-O(4)	1.9380(15)	Cu2-O(2)	1.9603(15)		
Cu1-O(1)	1.9400(15)	Cu2-O(5)	1.9708(15)		
Cu1-N(2)	1.9980(18)	Cu2-N(3)	1.9969(17)		
Cu1-N(1)	2.0208(18)	Cu2-N(4)	2.0095(19)		
Cu1-Cl(1)	2.5341(7)	Cu2-O(8)	2.066(5)		
		Cu2-Cl(2)	2.5611(14)		
O(4)-Cu(1)-O(1)	95.80(6)	N(2)-Cu(1)-Cl(1)	92.28(6)	O(2)-Cu(2)-O(8)	94.74(15)
O(4)-Cu(1)-N(2)	171.25(7)	N(1)-Cu(1)-Cl(1)	102.54(5)	O(5)-Cu(2)-O(8)	101.24(14)
O(1)-Cu(1)-N(2)	89.35(7)	O(2)-Cu(2)-O(5)	89.89(6)	N(3)-Cu(2)-O(8)	95.77(15)
O(4)-Cu(1)-N(1)	92.25(7)	O(2)-Cu(2)-N(3)	169.00(7)	N(4)-Cu(2)-O(8)	100.26(14)
O(1)-Cu(1)-N(1)	158.88(7)	O(5)-Cu(2)-N(3)	91.27(6)	O(2)-Cu(2)-Cl(2)	98.50(6)
N(2)-Cu(1)-N(1)	80.57(7)	O(2)-Cu(2)-N(4)	94.01(7)	O(5)-Cu(2)-Cl(2)	95.87(5)
O(4)-Cu(1)-Cl(1)	94.16(5)	O(5)-Cu(2)-N(4)	157.74(7)	N(3)-Cu(2)-Cl(2)	92.27(6)
O(1)-Cu(1)-Cl(1)	96.33(5)	N(3)-Cu(2)-N(4)	80.91(7)	N(4)-Cu(2)-Cl(2)	105.18(6)

Table S4. Hydrogen bonds for **1** (Å and °).

D-H…A	d(D-H)	d(H…A)	d(D…A)	<(DHA)
O(1)-H(1A)…O(9)	0.826(10)	1.867(12)	2.686(3)	171(3)
N(1)-H(1)…O(7)#1	0.88	1.76	2.640(3)	173.2
O(8)-H(8A)…O(6)	0.831(10)	1.844(12)	2.660(3)	167(3)

Symmetry transformations used to generate equivalent atoms:

#1 -x+1, -y+1, -z+1

Table S5. Hydrogen bonds for **2** (Å and °).

D-H…A	d(D-H)	d(H…A)	d(D…A)	<(DHA)
O(3)-H(3A)...O(3)#1	0.8399(11)	1.578(10)	2.408(3)	169(5)
O(7)-H(7A^a)...O(7)#1	0.844(10)	2.05(2)	2.845(3)	158(5)
N(5)-H(5)...O(5)#2	0.862(10)	1.861(11)	2.720(2)	175(3)
O(9^c)-H(9A^c)...Cl(1)#3	0.8400(11)	2.57(4)	3.214(9)	134(5)
O(9A^d)-H(9D^d)...O(5)	0.8400(10)	2.61(2)	3.334(6)	146(3)
O(9B^e)-H(9F^e)...O(6)#3	0.8400(11)	1.89(3)	2.708(17)	163(6)

Symmetry transformations used to generate equivalent atoms:

#1 –x+1, y, -z+1/2   #2 x, -y+1, z+1/2   #3 x, -y+1, z-1/2

Table S6. τ_5 values for Cu(II) centers in complexes **1** and **2**.

Complex	Center	τ_5
1	Cu1	0.18
	Cu2	0.21
	Cu3	0.14
	Cu4	0.07
2	Cu1	0.21
	Cu2	0.19

$$\tau_5 = \frac{(\alpha - \beta)}{60} \quad ; \alpha > \beta \qquad \text{Eq. (1)}$$

α and β being the largest valence angles of the coordination center.

τ_5= 0; square pyramidal, τ_5= 1; trigonal bipyramidal.

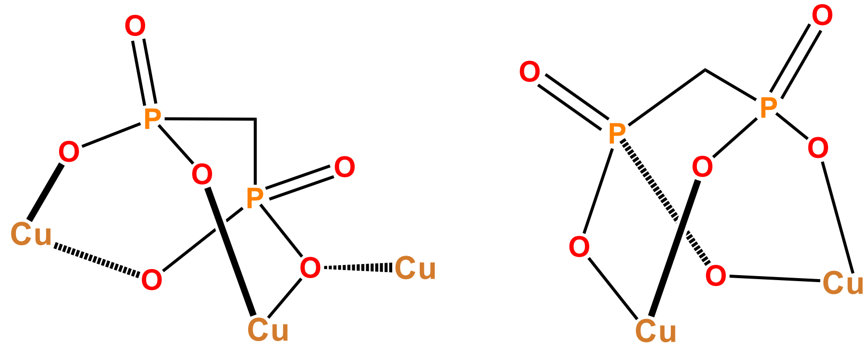

1 **2**

Fig. S1. Coordination mode of bisphosphonate in crystal structures of **1** and **2**.

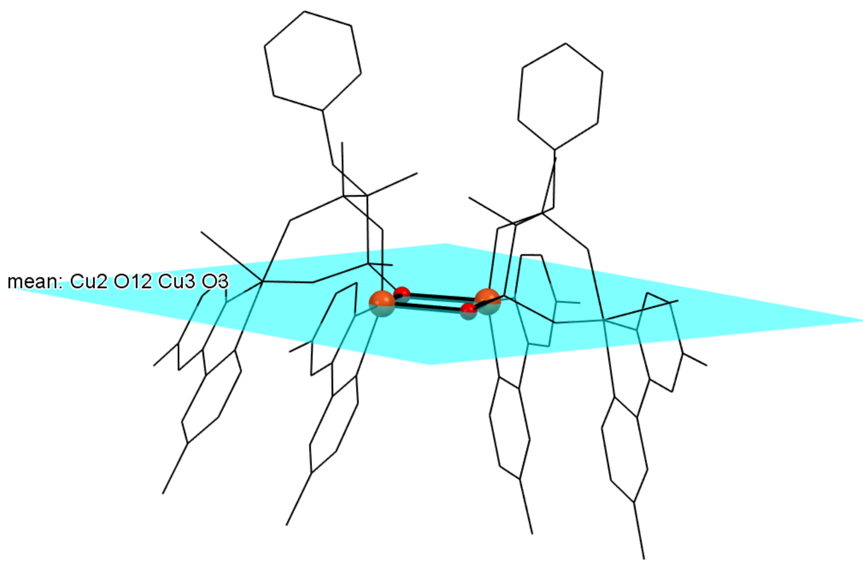

Fig. S2. Combinated molecular perspective in ball and stick/wireframe of crystal structure of **1** showing the four-membered ring.

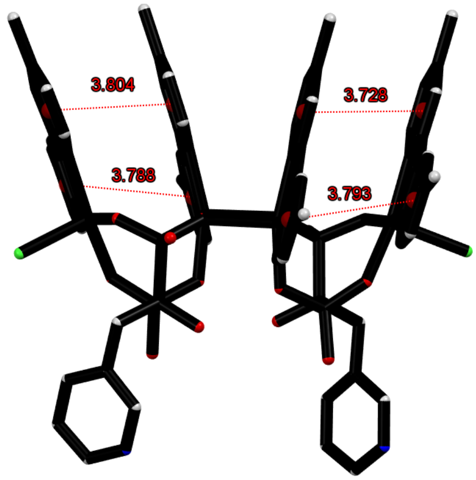

Fig. S3. Molecular perspective of crystal **1** in stick model showing the intramolecular distances π···π in red dashed lines. These distances were measured between the centroids of the aromatic rings from 4,4´-dmbp.

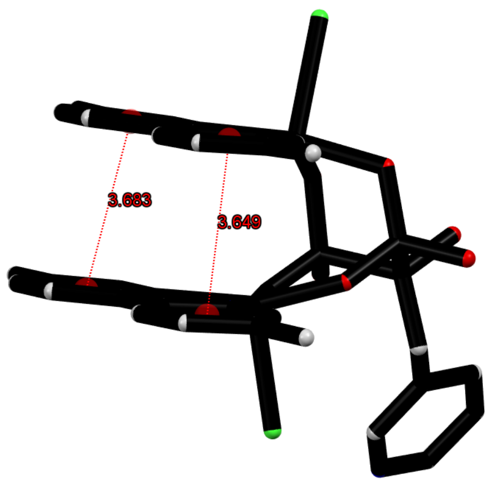

Fig. S4. Molecular perspective of crystal **2** in stick model showing the intramolecular distances π···π in red dashed lines. These distances were measured between the centroids of the aromatic rings from 5,5´-dmbp.

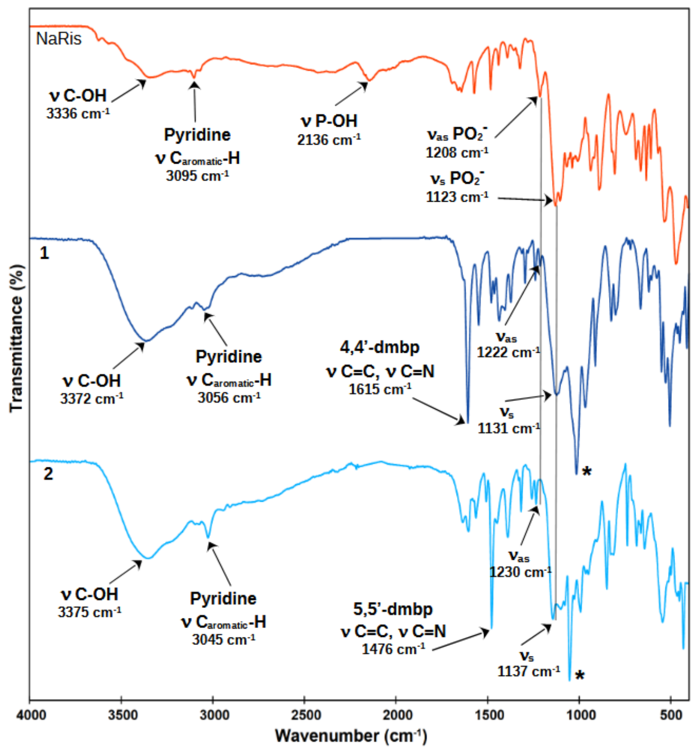

Fig. S5. ATR-IR (cm^{-1}) spectra of sodium risedronate (NaRis, top), [Cu_4(4,4'-dmbp)$_4$(HRis)$_2$$Cl_2$] (**1**, middle) and [$Cu_2$(5,5'-dmbp)$_2$(HRis)$_2ClH_2O$] (**2**, bottom). The spectra of **1** and **2** have a narrow band located at 1023 cm^{-1} for **1** and at 1045 cm^{-1} for **2**, these signals with black asterisks can be assigned to C-H rocking vibrations of the methyl substituents in 4,4'-and 5,5'-dmbp.

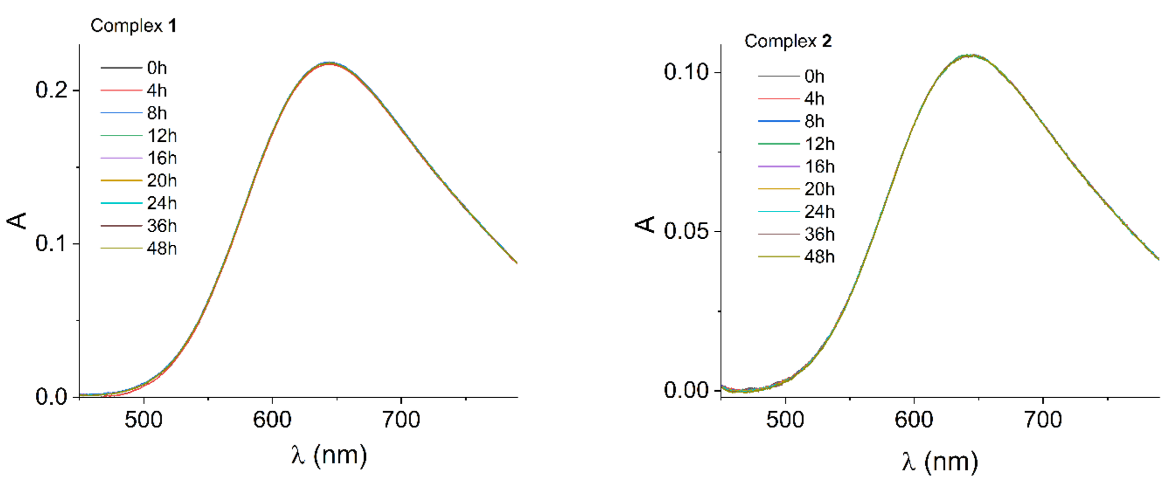

Fig. S6. UV-Vis spectra of aqueous solution of **1** (left) and **2** (right) (1.0 mM each one) at different time intervals up to 48 h.

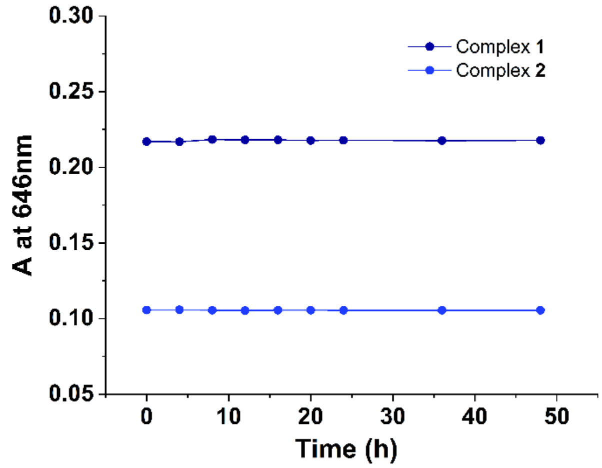

Fig. S7. Plot of absorption maxima (646 nm) *versus* time of aqueous solutions of **1** and **2** obtained from the spectra in Fig. S6.

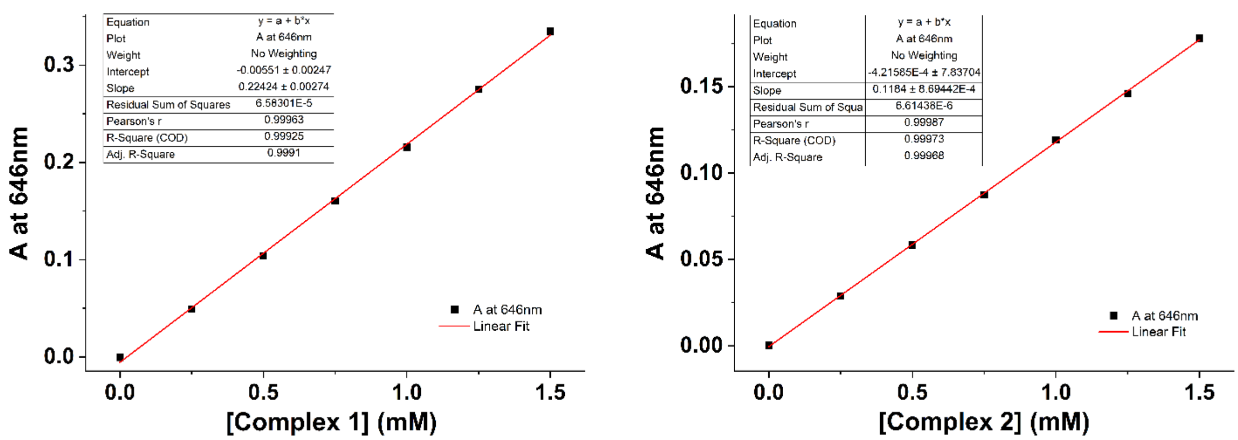

Fig. S8. UV-Vis calibration curves for the quantification of **1** (left) and **2** (right) in the aqueous phase.

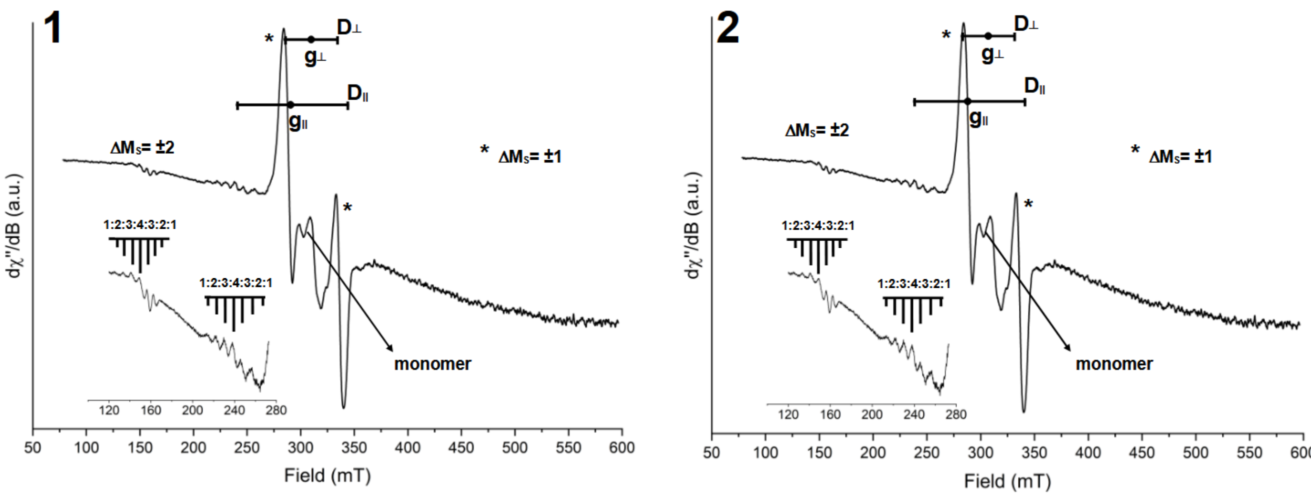

Fig. S9. X-band EPR spectra of **1** and **2** obtained in H_2O frozen matrix at 77 K. Monomer contribution to the spectra is marked for the signal located between the $\Delta M_S = \pm 1$ signals at 300 mT.

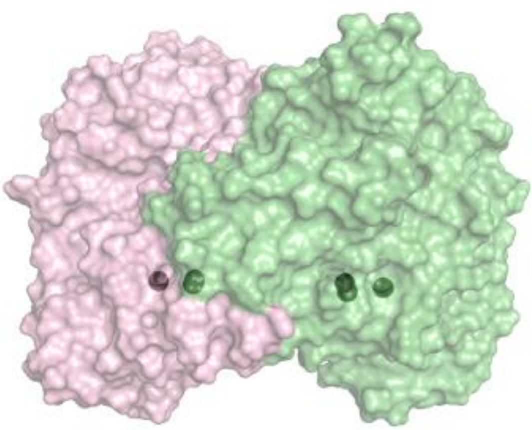

Fig. S10. 3D Representation of TcFPPS enzyme. The image shows that it is a dimer, monomers A (pink) and B (green) (1YHM). In each monomer, dark spheres represent three Mg^{2+} atoms located in the active site. Image obtained using: PyMOL (TM) 2.5.4 from Schrodinger, LLC.

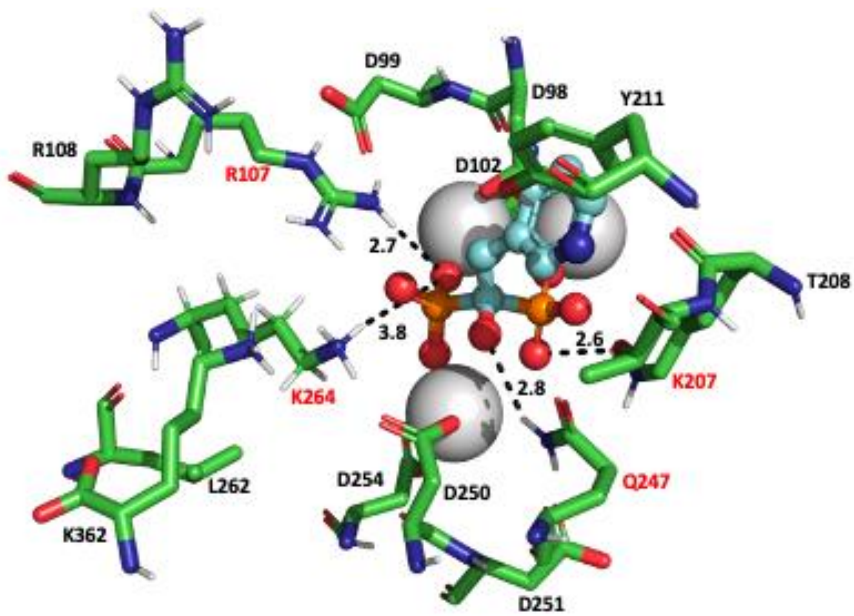

Fig. S11. 3D Risedronate–protein interactions. Black dotted line corresponds to hydrogen bond type interactions, distance of the bridges expressed in Å. The interacting residues with risedronate are depicted as red. Images obtained using: PyMOL (TM) 2.5.4 from Schrodinger, LLC.

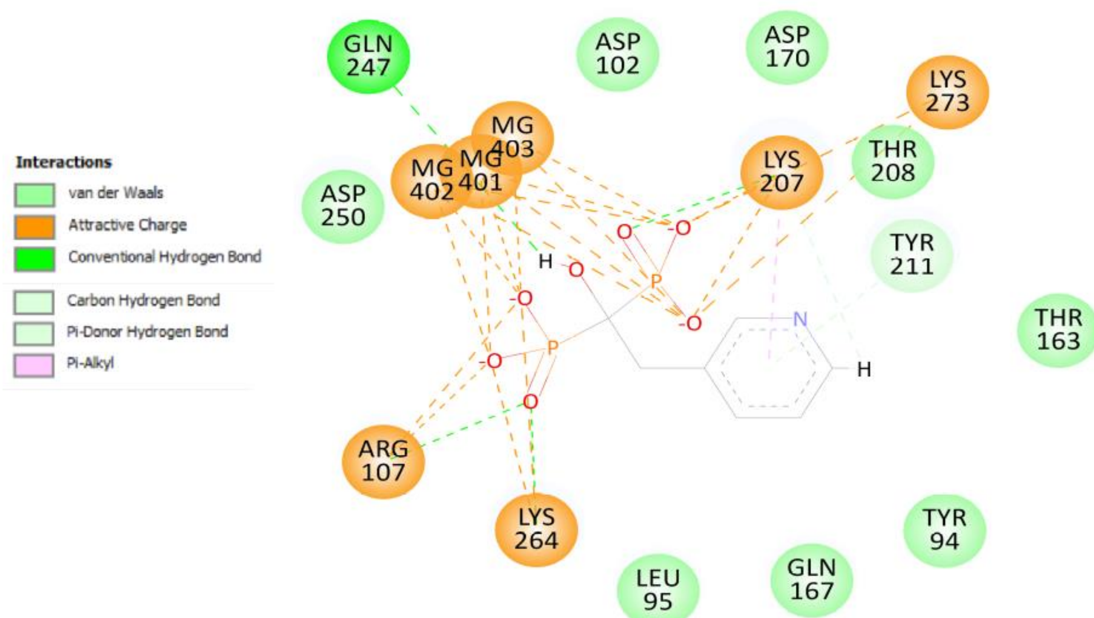

Fig. S12. 2D Risedronate–protein interactions. Electrostatic (van der Waals), pi-donor, pi-alkyl and carbon-hydrogen interactions are observed. The interactions (attractive charges between the ligand and the Mg^{2+} molecules) are key for the inhibition of the enzyme. Images obtained through: Biovia Discovery studio visualize 2021 v 21.1.0.